Fabrication of flexible silicon nanowires by self-assembled metal assisted chemical etching for surface enhanced Raman spectroscopy

ARTICLE

Fabrication of Flexible Silicon Nanowires by Self-assembled Metal Assisted Chemical Etching for Surface Enhanced Raman Spectroscopy

S. A. Kara[a,b,d], A. Keffous[b], A. M. Giovannozzi[*c], A. M. Rossi[c], E. Cara[d], L. D'Ortenzi[d], K. Sparnacci[e], L. Boarino[d], N. Gabouze[b] and S. Soukane[a]

A homogenous array of flexible gold coated Silicon nanowires was fabricated by the combination of Nano Spheres Lithography and Metal Assisted Chemical Etching to obtain highly effective Surface Enhanced Raman Spectroscopy (SERS) substrates. 3D nanostructures with different aspect ratios and well-defined geometries were produced by adjusting the fabrication parameters in order to select the best configuration for SERS analysis. The optimum flexible nanowires with an aspect ratio of 1:10 can self-close driven by the microcapillary force under exposure to liquid and trap the molecules at their metallic coated "fingertips", thus generating hot spots with ultrahigh field enhancement. The performance of these SERS substrates was evaluated using melamine as the analyte probe with various concentrations from the millimolar to the picomolar range. Flexible gold coated SiNWs demonstrated high uniformity of the Raman signal over large area with a variability of only 10% and high sensitivity with a limit of detection of $3.20*10^{-7}$ mg l^{-1} (picomolar) which promotes its application in several fields such food safety, diagnostic and pharmaceutical. Such an approach represents a low-cost alternative to the traditional nanofabrication processes to obtain well ordered silicon nanostructures, offering multiple degrees of freedom in the design of different geometries such as inter-wire distance, density of the wires on the surface as well as their length, thus showing a great potential for the fabrication of SERS substrates.

Introduction

Since its discovery in 1974, Surface Enhanced Raman Spectroscopy (SERS) [1-3] has become one of the most promising analytical tools to detect trace of chemical and biological species down to a single molecule level[4] in both liquid and gas phase [5-9]. Due to its specificity and sensitivity, SERS has gained a wide range of applications such as in electrochemistry, environmental analysis and bio-sensing [10-13]. Even if two substantially different primary theories, i.e. electromagnetic theory and chemical theory were developed to explain SERS mechanism, it is now generally agreed that SERS phenomenon is mainly based on the electromagnetic field enhancement. The enhancement results from the amplification of the light by the excitation of localized surface plasmon resonances (LSPRs) and occurs preferentially in the gaps, crevices, or sharp features of plasmonic materials, which are traditionally noble and coinage metals (e.g., silver, gold, and copper) with nanoscale features [14]. In particular, the so-called "Raman hot spots" are generated by the close proximity of metal nanostructures separated by a space of a few nanometers[15, 16]. Since the SERS effect strongly depends on the nanostructure of the supporting plasmonic material, much attention was paid to the fabrication of highly active SERS substrate with high degree of reliability and reproducibility [10, 17,18]. SERS substrates can be classified into three categories depending on their morphology: 1D, 2D and 3D. Most commonly used SERS nano-structured substrates include colloidal Ag/Au nano-particles (NPs) [19, 20], Ag/Au NPs array [21, 22] and Ag/Au nanowires or Ag/Au coated nanowires [23-29]. The fabrication of these substrates can be performed by different micro and nanofabrication approaches such as optical lithography [30], electron beam lithography (EBL) [31], focused ion beam (FIB) [32] and nano-imprint lithography (NIL) [33].

In the last years, new strategies were reported concerning flexible SERS substrates based on Au/Ag tips coated nanopillars which exploits a trapping molecules configuration[18,34-37] in order to achieve the minimum inter-distance gaps (less than 5 nm) between the active plasmonic materials. These flexible nanostructures can self-close driven by the microcapillary force under exposure to liquid and trap the molecules at their metallic coated apex or "fingertips", thus generating hot spots with an ultrahigh field

[a.] *Department of Chemical Engineering, Faculty of Technology, University of Blida 1, route de SOUMÂA B.P. 270, 09000* Blida*, Algeria.*
[b.] *Centre de Recherche en Technologie des Semi-conducteurs pour l'Energétique (CRTSE), Thin Films, Surface and Interface Division, 02, Bd. Dr. Frantz Fanon, B.P. 140, Alger-7 Merveilles, 16038 Algiers, Algeria.*
[c.] *Department of Quality of Life, INRiM, Strada delle Cacce, 10135, Turin, Italy.*
E-mail: a.giovannozzi@inrim.it
[d.] *Nanofacility Piemonte, National Institute of Metrologic Research (INRiM), Turin, Italy.*
[e.] *Dipartimento di Scienze e Innovazione Tecnologica, Università del Piemonte Orientale "Avogadro", INSTM, UdR Alessandria, Viale T. Michel 11, Alessandria, Italy.*
†Electronic Supplementary Information (ESI) available: See
DOI: 10.1039/x0xx00000x

enhancement. In fact, the inter-gap distance between the plasmonic nanostructures is determined by the size of the molecule that sits within the fingertips. Hu and co-workers reported gold coated flexible polymer fingers fabricated by a combination of EBL, reactive ion etching (RIE) and NIL [35], achieving a nanometer precision in the control of the gap size between plasmonic structures with reproducible hot spots. However, this method requires very expensive instrumentation and it suffers the main limitation of EBL in terms of fabrication over large area. Recently, Schmidt and co-workers proposed a simpler and cheaper method based on mask-less dry etching to produce flexible silver coated silicon nano-pillars on large area [36]. This method demonstrated high uniform field enhancement of the SERS signal across the surface but the requirement of sophisticate instruments for standard silicon processing still remains.

The development of simple and low-cost methods for the machining of high aspect ratio nanostructures on large area with equipment available in most research institutions is therefore required [37]. Nano-spheres lithography (NSL), based on the self-assembly of polymer or metal nano-spheres as a surface patterning method [33,38,39], in combination with Metal Assisted Chemical Etching [40] (MACE), represent good candidates for cost-effective fabrication of large-scale orderly functional nanostructure arrays [41,42]. MACE is an anisotropic wet etching technique, which is catalyzed by the presence of noble metal (the most frequently used are Ag, Au, Pt and Pd) film on a silicon wafer. It offers the possibility to obtain high aspect ratio nanostructures whose geometry strictly depends on the surface metal distribution, on the concentration of the etching solution and on the total time of etching [43]. Recently, silicon nanowires (SiNWs) were employed as supporting SERS substrates due to their unique optical, electrical and mechanical proprieties [44-46]. SiNWs offer large area to volume ratios and they have the ability to confine the incident light on their surface, improving the light conversion and, consequently, the enhancement of the localized electromagnetic field[47-50]. Moreover, the mechanical properties of silicon offer the possibility to have robust and flexible free-standing wires.

Herein, we report a fabrication method based on the combination of Nano Spheres Lithography (NSL), as a large-area surface patterning technique, and MACE, to achieve well-defined flexible Au-coated cylindrical SiNWs to support Surface Enhanced Raman Scattering. Our approach constitutes a low-cost alternative to EBL and RIE in the fabrication of ordered matrix of SiNWs, offering multiple degrees of freedom in design and fabrication of SERS substrate, ranging from the micro to the nanoscale. Different 3D nanostructures can be fabricated by adjusting NSL and MACE parameters in order to change the inter-wire distance, the density of the wires on the surface as well as their length. SERS efficiency of these substrates was investigated in different “leaning” and “non leaning” wires configurations in order to select the optimum configuration for Raman analysis. Melamine (Mel) was used as the test analyte to evaluate the performance of the SERS substrate in terms of uniformity of the Raman signal across large area, sensitivity of the SERS substrate for analyte detection and analytical enhancement factor. Mel was recently involved in food scandals because it was fraudulently added in milk, pet and animal feed to increase the apparent content of protein, causing kidney failures and even death in infants in China [51].Therefore, the performance of this SERS substrate was also evaluated in terms of food safety applications.

Experimental

Materials and chemicals

Silicon wafer n+ type with resistivity of 27-47 mΩ cm were provided by SunEDISON/MEMC. Styrene was purchased from Sigma-Aldrich and purified by passing through an inhibitor removal column (Sigma-Aldrich) before use. Sodium dodecyl sulfate (SDS), potassium persulfate (KPS) and Melamine (99%) were purchased from Sigma-Aldrich and used without further purification. Hydrochloric acid (HCl 37%), Sulfuric acid (HSO_4 96%), Hydrofluoric acid (HF 50%), Hydrogen Peroxide (H_2O_2 30%), absolute Ethanol (99,99%) and Acetone (>99.5%) were obtained by Carlo Erba Reagents (Rodano, Italy). All solutions were prepared with Milli-Q quality water (18 MΩcm). Piranha solution was prepared with $H_2SO_{4\,(96\%)}$: $H_2O_{2\,(30\%)}$ = 3 : 1 volume ratio. The etching solution of $HF_{(50\%)}$: $H_2O_{2\,(30\%)}$: H_2O with 3 : 1 : 1 ratio in volume was prepared and stored up to one month. Ethanol, acetone and de-ionized (DI) water were used to rinse the samples in many steps of the fabrication.

Synthesis of Polystyrene (PS) nano-spheres

The polystyrene nanoparticles were synthesized by emulsion polymerization. The polymerization reactions were carried out in a 1 L five-neck equipped with a condenser, a mechanical stirrer, a thermometer and inlets for nitrogen and styrene. 500 ml of deionized water containing 0.3 g (1.0 mmol) of SDS were introduced into the reactor at room temperature with a stirring rate of 300 rpm, and then 70.0 ml (0.61 mol) of styrene were added dropwise. The mixture was purged with nitrogen, and nitrogen was fluxed during the entire polymerization procedure. The reactor was heated to 80 °C, then a potassium persulfate aqueous solution (5.0 ml, 0.74 mmol) was added, and the mixture was reacted for 24 h. The obtained latex was purified from surfactant and unreacted monomer by repeated dialyses against water (cellulose membrane, molecular weight cut-off 12 kDa). The polystyrene nanoparticle size, determined by electron microscopy, was 250 ± 4 nm while the hydrodynamic radius, determined by dynamic light-scattering (DLS) was 259 nm (PDI 0.020).

Silicon nanowires fabrication

Silicon nanowires were fabricated by nanospheres lithography and MACE. The first step consisted in cutting and cleaning square silicon substrates (1.5 cm per side) using acetone and ethanol, the surface functionalization was performed by piranha solution at 80°C for 90 minutes to render the surface hydrophilic. The sample was then abundantly rinsed with DI water and we deposited 60 µl of a

colloidal aqueous solution of PS beads with diameter of 260 nm by spin coating, the consequent self-assembly process leads to a monolayer of nanospheres in hexagonally close-packed (hcp) configuration. The homogeneity of the monolayer depends on the spinner parameters and the quality of nanospheres colloidal solution; we performed spin coating in two steps, set as follows: step 1: vel. = 500 rpm, acl. = 400 rpm/s, time = 10 s; step 2: vel. = 3000 rpm, acl. = 1000 rpm/s, time = 30 s. Subsequently, we reduced the spheres size by means of an etching process using Ar^+ plasma (Dibiscom Plasma Matrix, RF power = 75 W, time = 8 minutes and pressure = 10^{-2} mbar). The following step consisted in the deposition of a thin gold film (20 nm) by e-beam evaporation, the reduced nanospheres in hexagonally non-close-packed configuration acted as a mask, so by removing them in an ultrasonic bath of ethanol, we obtained a gold film patterned over the whole surface with a two dimensional array of circular. We proceeded by transferring this geometry to the bulk silicon by the MACE technique.

MACE can be described as a sort of self-catalytic etching of silicon and other semiconductor, where the formation mechanism is ruled by local redox potential of the metal with respect to the semiconductor in the presence of hydrofluoric acid and an oxidizing agent. This drives the holes necessary to dissolution at the metal-semiconductor interface. In the case of silicon, the metal at the interface rapidly sinks following the crystallographic directions, and defines silicon walls or wires, depending on the metal distribution at surface, on the temperature and concentration of the etchants. The reaction mechanisms involved in the dissolution of silicon in the etching solution are rather complex and are descript in details in the work of Chartier and coworkers[52] for the case of Ag on Si.

In our procedure, we soaked the sample in the etching solution for 40 to 60 seconds and stopped the process by rinsing the sample with ethanol. The final process to prepare the sample for SERS application is the coating of the matrix of silicon nanowires with 80 nm of gold which we deposited by e-beam evaporation.

Scanning Electron Microscopy analysis

A morphological characterization has been carried out using FEI Inspect-F™ Field Emission Gun scanning electron microscope (FEG-SEM); we used 10 kV to observe PS nanospheres and up to 30 kV for gold structures and silicon nanowires with secondary electrons detector. We always adopted a 30° tilted configuration which enables the cross-sectional view of the nanostructures and we varied magnification from 20,000 times to 120,000 times depending on the features size.

Raman analysis

Different concentrations of Mel solution ranging from 100 mg l^{-1} to $1*10^{-5}$ mg l^{-1} were prepared in Milli-Q water by a serial dilution of a Mel stock solution at 1000 mg l^{-1}. A 1 µl droplet of the different Mel aliquots were deposited onto the SERS substrate and let them dry in air before Raman characterization. All Raman spectra were recorded using a Thermo Scientific DXR Raman equipped with a microscope, an excitation laser source at 780 nm with a motorized stage sample with a minimum step size of 1 µm equipped with a charge-coupled device (CCD) detector. Spectra of melamine samples on SiNWs substrates were collected using a 10x microscope objective, a 50µm slit aperture and a spectral range from 400 cm^{-1} to 3500 cm^{-1} with a grating resolution of 5 cm^{-1} and with a 24mW laser excitation power. The acquisition time was of 20s with 1s exposure time. Raman mapping were performed on all tested substrates using the same collection parameters on an area of 4x4 mm using a step size of 150 µm.

Results and discussion

Silicon Nanowires characterization

The adopted fabrication procedure gave a SiNWs matrix which can be tested with SERS active molecules, the results of each step of fabrication are shown in Figure 2. At first, we were able to achieve an extended monolayer of self-assembled PS nanobeads presenting some linear and punctual defects which results in the presence of domains of some micrometres (Fig. 2a). The reduction of the nanospheres size by plasma etching allows an accurate control of the final diameter of the nanospheres, ranging from 100 to 130 nm by appropriately setting the duration of the process (Fig. 2b). By changing the original nanobeads, the spheres spacing can be set as well, consequently leading to wide variability of the geometrical features of the nanostructures. After plasma etching, gold deposition and nanospheres removal, we obtained an hcp ordered pattern of circular holes on the metallic film, the so-called "antidot" mask (Fig. 2c) which assists the successive etching process. The etching rate depends on the type and doping level of bulk silicon, on the relative concentration of HF and H_2O_2 in the etching solution as well as on the spacing between consecutive antidots [39]. During etching at room temperature, the length of SiNWs varies linearly with the etching time [53] so that a fine control of this parameter can be achieved by changing the time of etching.

Once the etching is completed, a gray stain appears on the bulk silicon, caused by the reduction of the reflectance due to the nanostructured surface [54]. Thus, we obtained a matrix of standing silicon nanowires (Fig. 2d) with diameter ranging from 100 to 130 nm and different lengths, varying from 600 nm to 1.3 µm. The ultimate substrates for SERS analysis consist of SiNWs with gold caps on top (Fig. 2e) covering the diameter of the nano-wires; the gold thickness was chosen to be 80 nm in order to ensure the maximum intensity in correspondence to a laser excitation wavelength of 785 nm (see Raman measurements paragraph).

The optimization of the etching conditions (time, solution concentration) allowed us to exploit the mechanical properties of SiNWs by fabricating wires with different lengths. When the SiNWs have aspect ratios (ratio of diameter and length) larger than 1:10, they bend and stick together to from bundles during drying, after liquid etching (Fig. S1a, see supplementary information). On the other hand, SiNWs with aspect ratio of 1:10 remain straight during and after fabrication, as shown in Fig. 2d. Moreover, straight SiNWs with aspect ratio of 1:5 were fabricated (Fig. S1b, see supplementary information).

In order to demonstrate whether the resulting standing SiNWs are flexible and able to bend or not, we performed the following test, illustrated in (Figure 3a), we exposed substrates with long (aspect ratio 1:10) and short (aspect ratio 1:5) SiNWs to a droplet of water and let them dry in the air. After water evaporation we noticed that the SiNWs with aspect ratio 1:10 leaned and stick together forming different bundles of wires (Fig.3b), while the SiNWs with aspect ratio 1:5 remain straight exhibiting high stiffness (Fig. S1b). A similar test was also conducted with a droplet of Ethanol. No leaning phenomenon was observed. Thus, the leaning phenomenon could be explained by the capillarity effects during drying, due to the surface tension of the water. In addition, it has been demonstrated that the elastic modulus of silicon nanowires is independent of their diameters, if the diameter is larger than 100 nm; this supports that finite size effect (due to surface tension) does not play a role on elastic behaviour of silicon nanowires with diameter of >100 nm [53].

The leaning effect allowed us to have a large number of bundles of nano-wires in the area corresponding to the droplet size on the substrate while no leaning is visible outside the drop area, as shown in (Fig. 3b). It is assumed that a hot-spot is created at the tip-to-tip site between two leaning nanowires and thus a large number of electromagnetic hot spots are present on the substrate (Figure S2, see supplementary information). The combined use of NSL and MACE for SiNWs fabrication guaranteed a good control over the geometrical parameters, such as diameter and centre-to-centre distance, and manufacturing over large areas as well as large aspect ratios, which could be difficult to obtain by EBL and RIE, respectively. The aspect ratio of silicon nanostructures is indeed a very crucial parameter as well as the position of the analyte with respect to the hot-spots; both these parameters have been widely investigated to find the most convenient configuration for the enhancement of Raman scattering as treated in the following section.

Raman Measurements

It was previously demonstrated that the leaning of flexible nanostructures such as nanofingers [33] or nanopillars [36] coated with silver or gold is crucial for the intensity Raman enhancement. As already mentioned in Fig.3, the flexibility of the free standing silicon nanowires here presented strongly depends on the length of the wires whose leaning properties are impaired when a wire's length is shorter than 0.6 um. In order to demonstrate that the SERS effect is magnified when flexible SiNWs are used due to entrapment of the analyte in a multiple hot spots configuration, a SERS comparison test between leaning and non-leaning nanowires was initially performed (Fig.4). Moreover, the pre-leaned wires, i.e. wires brought to lean before the deposition of the analyte, and post leaning wires, wires brought to lean during the deposition of the analyte, were also compared to better understand the efficiency of the SERS mechanism. SiNWs substrates with an aspect ratio of 1:5 and 1:10 were chosen for the so-called "non leaning wires" and "leaning wires" samples, respectively. In the "pre-leaned wires" configuration a drop of pure water was first deposited on the SiNWs substrate to induce the leaning of the nanowires before the addition of the analyte probe. In these tests melamine (Mel) molecule was chosen as analyte probe thanks to the demonstrated properties to bind the gold surface [55,56], thus it is an ideal candidate to investigate the SERS mechanism occurring on the SiNWs based substrate. A droplet of 100 mg l^{-1} Mel solution was deposited on leaning and non-leaning SiNWs samples and let it dry in air before Raman analysis.

In Fig.4 typical Raman peaks of solid melamine at 380 cm^{-1}, 580 cm^{-1}, 678 cm^{-1} and 983 cm^{-1} are shown. The most intense peak at 676 cm^{-1} is assigned to the ring-breathing II mode, which involves the in-plane deformation of the triazine ring. The second most intense peak at 983 cm^{-1} arises from the ring-breathing mode I of the triazine ring [54]. As Fig.4 shows, the SERS spectra of melamine are dominated by the amine trigonal breathing mode which shifts at higher wavenumbers and splits into two main peaks at 680 cm^{-1} and 712 cm^{-1}, indicating that melamine is bound to the electropositive gold surface via the lone electron pair of ring nitrogen. Remarkable splitting and shifts of 10 cm^{-1} and 40 cm^{-1} from the original melamine bands at 676 cm^{-1} were already reported in the literature using respectively Klarite SERS substrates [58], triangular shape gold nanoparticles [59], silver nano-particles [54] and spherical gold nanoparticles [60]. It is reasonable to infer that a strong polarization occurs at the surface of these metallic nanostructures and where the electric field strongly increases, it can result in not only an increased enhancement factor, but also in a change of the vibrational Raman selection rules, which allows the appearance of forbidden Raman bands. Moreover, the shift and the relative intensity ratio between the main peaks at 680 cm^{-1} and 712 cm^{-1} depend on the physiochemical interactions of the melamine with the metallic nanostructures and on the different hot spots configuration at the surface of the SERS substrates. When the melamine is deposited on the "non leaning wires" sample, it is assumed that the analyte adsorbs uniformly all over the gold coated tips of the nanowires, leading to an enhancement of the Raman signal of the melamine. In particular, as reported by Wu et al.[61], when free standing wires i.e. "non leaning wires" are present on the surface and the Raman excitation is provided by a 780nm laser line, we could infer that a strong enhancement of the electric field occur at the interface Au/SiNWs. In this hot spots configuration the ring-breathing II mode is dominated by the peak at 680 cm^{-1}, which reaches about 1000 counts/sec with only a small shoulder at 712 cm^{-1}. Remarkable shifts of the traditional melamine Raman bands at 580 cm^{-1} and 983 cm^{-1} to 600 cm^{-1} and 1000 cm^{-1} were also registered, respectively, together with the first order of silicon at 520 cm^{-1}. When clustered wires i.e. "leaned wires" are present on the surface, instead, a strong local electromagnetic field should be mainly distributed in the gaps between the Au particles with the formation of multiple hot spots. Melamine molecules are adsorbed at the gold coated tips of the wires and entrapped in clustered Raman hot spots with the smallest spacing between the nanowires tips determined by the analyte molecule size. The formation of multiple hot spots after the leaning of the wires resulted in a huge enhancement of the melamine signal at 712 cm^{-1} which reaches

about 4000 counts/sec for "pre-leaned wires" and 9000 counts/sec for "post-leaned wires" configurations, respectively (Fig.4). The first order of silicon at 520 cm^{-1} is clearly visible in the "pre-leaned wires" but partially overlapped with a Mel peak in the "post-leaned wires" due to the huge Raman enhancement of the melamine signal. This means that if the wires are brought to lean before the deposition of the analyte (pre-leaned), the Raman signal from pre-leaned wire is approximately 2 times lower than from the post-leaned wires. This indicates that some potential hot spots and/or adsorption sites are forbidden by leaning prior to analyte exposure. These results well agree with what already reported in literature [33] with post-leaned wires configuration showing the highest enhancement factor respect to pre-leaned wires and non leaning wires configurations. In case of optimum SiNWs for SERS, i.e. 1:10 aspect ratio SiNWs with a diameter from 100 - 130 nm, the inter-wires distance is about 100 nm and it depends on the dimensions of the starting PS spheres (260 nm). Gold caps with different thicknesses at 40 nm, 60 nm and 80 nm were tested in SERS measurements (data not shown). SiNWs with a gold cap of 80 nm provided the highest enhancement in Mel SERS measurements, which well agrees to what already reported in literature by Ou et al.[18], where a gold thickness of 80 nm was used on flexible polymer fingers to ensure the maximum intensity in correspondence to a laser excitation wavelength of 785 nm. Thicknesses higher than 80 nm were not tested to avoid the risk of getting a continuous film of gold between adjacent SiNWs, which might affect the SERS efficiency of the substrate. Higher gold thicknesses could be tested by changing the dimensions of the starting PS spheres in order to increase the inter-wires distance.

SiNWs with aspect ratio of 1:10 used in "Post-leaned configuration" were then selected for the further characterization of the performance of the SERS substrate. In particular, the uniformity of the Raman signal across the area of leaning nanowires, the sensitivity of the SERS substrate in terms of analyte detection and the analytical enhancement factor were studied.

In order to study the uniformity of the Raman signal across an area of leaning nanowires, a 1 µl droplet of 100 mg l^{-1} Mel solution was deposited on the substrate and Raman mapping was performed on the entire area covered by the evaporated droplet. An area of approx 4x4 mm was mapped with a micro Raman system using a laser spot size of 3.1 µm in diameter and a step size of 150 µm obtaining 756 spectra in total (Fig. 5a). Fig. 5b shows the resulting Raman map obtained by plotting the area of the specific Mel peak in the spectral range 750 cm^{-1} – 650 cm^{-1} over the scanned surface with a color scale bar from blue to red that provides semi-quantitative analysis. As (Fig. 5c) shows, the distribution of the Mel signal on the SERS substrate is only confined in the droplet region with a good homogeneity distribution from the centre to the edge of the stain. The investigated Mel signal at 712 cm^{-1} is relatively uniform within the leaned nanowires area and a 10% deviation from the average signal across the leaned area was calculated.

Since the SERS substrate based on post-leaned SiNWs provided a good homogeneity of the Mel Raman signal across the droplet region, we decided to investigate the dynamic range of the substrate in order to obtain a calibration curve for the melamine quantification and to detect the sensitivity limit for this molecule. Different concentrations of Mel solution ranging from 100 mg l^{-1} to $1*10^{-5}$ mg l^{-1} were deposited on the SiNWs substrates and characterized by Raman mapping after the post-leaned wires configuration was induced by solvent evaporation. At least 50 spectra were collected and used for statistical analysis. An average relative standard deviation of 10% of the Raman signal at 712 cm^{-1} was calculated for each concentration value. Average Raman spectra of each Mel concentration are reported in Figure 6. As(Fig. 6a) shows, very low concentrations of melamine such as $1*10^{-5}$ mg l^{-1} and $1*10^{-3}$ mg l^{-1} can be easily detected and distinguished from the blank signal (0 mg l^{-1}) but it is not possible to discriminate between them in this range of concentrations. The intensity of the ring-breathing II mode at 712 cm^{-1} tends to increase proportionally with the Mel concentration in the range from $1*10^{-3}$ mg l^{-1} to 1 mg l^{-1} but it starts to decrease when concentrations higher than 1 mg l^{-1} are used.

This behavior is quite common in SERS measurements and it is related to the saturation of the surface coverage of the metallic nanostructures as well as the hot spots regions which mainly contribute to the Raman enhancement. Since the highest intensity of the signal at 712 cm^{-1} is recorded with the melamine concentration of 1 mg l^{-1}, we can infer that the surface coverage of the gold coated tips by this melamine concentration could be approximated to a quasi monolayer morphology, which represents the best condition for the enhancement of its Raman signal. However, when higher concentrations of analyte are used (10 mg l^{-1} and 100 mg l^{-1}), Mel molecules accumulate at the top of the gold coated tips leading to the formation of thicker layers of analyte on the surface. The presence of few layers of Mel on top of the substrate reduces the amount of excitation photons that reach the Mel - gold coated SiNWs interface, inducing both a decrease of the intensity of the SERS peak at 712 cm^{-1} and an increase of the classical Raman band around 680 cm^{-1}.To exclude any effect due accumulation of the analyte by the coffee stain effects we perform test measurement by dipping the SiNWs substrate in a melamine solution. The behavior was confirmed by the immersion tests where the SiNWs substrates were dipped in Mel solutions at 1 mg l^{-1}, 10 mg l^{-1} and 100 mg l^{-1} for 20 minutes, thoroughly washed with water to remove the non-adsorbed molecules and let them dry in air before Raman analysis (Fig. S3, see supplementary information). In this case a slightly increase of the Raman intensity at 712 cm^{-1} was registered in the immersion tests by increasing the concentration of Mel (Fig. S3).

This means that the signal at 712 cm^{-1} is generated by a similar amount of Mel molecules adsorbed on the gold coated tips. Since the non-adsorbed Mel molecules were removed by intensively wash the substrate after the soaking procedure, they cannot block the excitation photons to reach the Mel - gold coated wires interface thus resulting in a slightly increase of the signal at 712 cm^{-1} but not in a decrease of the SERS signal. These observations further confirmed our hypothesis that the deposition of Mel concentrations higher than 1 mg l^{-1} by drop coating induces a

decreased efficiency of the SERS effect due to both the saturation of the clustered hot spots within the wires and the accumulation of few layers of non-adsorbed analyte molecules on the top of the substrate. Even if this phenomenon could affect the quantification of the Mel in the range of concentrations that was investigated, the relative intensity ratio between the specific Mel peaks at 680 cm^{-1} and 712cm^{-1} can be exploited for the building of a calibration curve and to provide a quantitative analysis of the Mel on the substrate. As (Fig. 6b) shows, after normalization of the Raman spectra to the intensity of the peak at 712 cm^{-1}, the intensity ratio at 680 cm^{-1} tends to increase proportionally with the melamine concentration.

A calibration curve was built in the range of concentrations between $1*10^{-8}$ mg l^{-1} - 10 mg l^{-1} by plotting the logarithm of relative intensity ratio at 680 cm^{-1} with the logarithm of Mel concentration (Fig.7). A linear regression model was applied for the calibration and the forcefulness of the fit was confirmed by the reduced chi-square value (i.e. the sum of the weighted squared residuals normalized by the number of degrees of freedom) which is attested close to 1 (Fig. 7).

The limit of detection (LOD) was experimentally detected on blank samples (n=10) and calculated by the equation:

$$LOD = M + 3s \quad (1)$$

Where *M* is the mean value of the relative intensity ratios at 680 cm^{-1} of the blank sample and *s* is the standard deviation.

The limit of quantitation (LOQ) was estimated with the following equation:

$$LOQ = 3.3*LOD \quad (2)$$

According to equations (1) and (2) the LOD and LOQ were $3.20*10^{-7}$ mg l^{-1} and $1.00*10^{-6}$ mg l^{-1}, respectively. The present methodology is then suitable for melamine quantification in the concentration range of $1.00*10^{-6}$ mg l^{-1} - 10 mg l^{-1} in accordance with the European law limits of 1 mg l^{-1} and 2.5 mg l^{-1} in dairy products for infants and other food and animal feed, respectively [62].

In order to complete the characterization of the SERS substrate based on SiNWs the enhancement factor (EF) was calculated.

The EF is usually calculated using (3), where $\square_{SERS}$ and $\square_{NR}$ are the intensity of the vibrational peak in SERS and normal Raman (NR) measurements, respectively, and $\square_{NR}$ and $\square_{SERS}$ are the concentration of the analyte probe in NR measurements and the SERS measurements, respectively:

$$EF = \frac{I_{SERS} C_{SERS}}{(1 + I_{NR}) C_{SERS}} \quad (3)$$

In order to determine the EF on the SiNWs SERS substrates, a 1 µl droplet of 1 mg l^{-1} Mel solution was deposited onto the gold coated SiNWs SERS substrate prepared with optimized conditions. Bare SiNWs substrate without the layer of gold on top was used as reference for traditional Raman measurement and spotted with the same amount of Mel on the surface. As (Fig.S4, see the supplementary information) shows, Mel is easily detected on the SiNWs SERS substrate with the main peaks at 1000 cm^{-1},712 cm^{-1}, 680 cm^{-1}, 600 cm^{-1} and 380 cm^{-1}. No Mel signal is revealed on the bare SiNWs and only the first and second order of Silicon at 520 cm^{-1} and around 1000 cm^{-1} are registered in the Raman spectrum, respectively. Applying the (3), assuming that $\square_{NR}$ and $\square_{SERS}$ are the same and using as $\square_{SERS}$ the intensity of the peak at 712 cm^{-1}, the EF was determined to be $1.3*10^4$. This number proved the efficiency of this SERS substrate and promotes its application in several fields such food safety, diagnostic and pharmaceutical.

Conclusions

In this work, a homogenous array of flexible gold coated SiNWs was obtained combining Nano Spheres Lithography and Metal Assisted Chemical Etching to support Surface Enhanced Raman Scattering. NLS was used as surface patterning method to obtain ordered self assembled nanostructures on large area, while MACE guaranteed high aspect ratio nanostructures with a well defined geometry. 3D nanostructures with different aspect ratios were produced by adjusting the fabrication parameters in order to change the flexibility of the wires and, consequently, to find the optimum condition for SERS analysis. Among the different configurations tested, the optimum flexible nanowires with an aspect ratio of 1:10 can self-close driven by the microcapillary force under exposure to liquid and trap the molecules at their metallic coated "fingertips", thus generating hot spots with ultrahigh field enhancement.

Melamine molecule was used as analyte probe to test the performance of this SERS substrate in terms of uniformity of the Raman signal across large area, sensitivity of the SERS substrate for analyte detection and analytical enhancement factor evaluation. Flexible gold coated SiNWs demonstrated high uniformity of the Raman signal over large area with a variability of only 10% and a high sensitivity of melamine detection with a LOD of $3.20*10^{-7}$ mg l^{-1} (picomolar) and an EF of $1*10^4$. Such approach represents a low-cost alternative to EBL and RIE in the fabrication of well ordered silicon nanostructures, offering multiple degrees of freedom in the design of different geometries such as inter-wire distance and density of the wires, thus showing a great potential for the fabrication of SERS substrates.

Acknowledgements

"*The project 15HLT01 MetVBadBugs has received funding from the EMPIR programme co-financed by the Participating States and from the European Union's Horizon 2020 research and innovation programme*".

Nanofacility is a laboratory funded by the "Compagnia di San Paolo" foundation.

Notes and references

1. M. Fleischmann, P. J. Hendra and A. J. McQuillan, *Chemical Physics Letters*, 1974, **26**, 163-166.
2. D. L. Jeanmaire and R. P. Van Duyne, *Journal of Electroanalytical Chemistry and Interfacial Electrochemistry*, 1977, **84**, 1-20.
3. M. G. Albrecht and J. A. Creighton, *Journal of the American Chemical Society*, 1977, **99**, 5215-5217.
4. K. Kneipp, Y. Wang, H. Kneipp, L. T. Perelman, I. Itzkan, R. R. Dasari and M. S. Feld, *Physical Review Letters*, 1997, **78**, 1667-1670.
5. S. S. R. Dasary, A. K. Singh, D. Senapati, H. Yu and P. C. Ray, *Journal of the American Chemical Society*, 2009, **131**, 13806-13812.
6. J. F. Li, Y. F. Huang, Y. Ding, Z. L. Yang, S. B. Li, X. S. Zhou, F. R. Fan, W. Zhang, Z. Y. Zhou, Y. WuDe, B. Ren, Z. L. Wang and Z. Q. Tian, *Nature*, 2010, **464**, 392-395.
7. Y. He, S. Su, T. Xu, Y. Zhong, J. A. Zapien, J. Li, C. Fan and S.-T. Lee, *Nano Today*, 2011, **6**, 122-130.
8. A. Chou, E. Jaatinen, R. Buividas, G. Seniutinas, S. Juodkazis, E. L. Izake and P. M. Fredericks, *Nanoscale*, 2012, **4**, 7419-7424.
9. V. K. K. Upadhyayula, *Analytica Chimica Acta*, 2012, **715**, 1-18.
10. M. Fan, G. F. S. Andrade and A. G. Brolo, *Analytica Chimica Acta*, 2011, **693**, 7-25.
11. G. McNay, D. Eustace, W. E. Smith, K. Faulds and D. Graham, *Appl. Spectrosc.*, 2011, **65**, 825-837.
12. L. Zhang, C. Jiang and Z. Zhang, *Nanoscale*, 2013, **5**, 3773-3779.
13. S. Gajaraj, C. Fan, M. Lin and Z. Hu, *Environmental Monitoring and Assessment*, 2013, **185**, 5673-5681.
14. B. Sharma, R. R. Frontiera, A.-I. Henry, E. Ringe and R. P. Van Duyne, *Materials Today*, 2012, **15**, 16-25.
15. M. Moskovits, *The Journal of Chemical Physics*, 1978, **69**, 4159-4161.
16. J. J. Baumberg, T. A. Kelf, Y. Sugawara, S. Cintra, M. E. Abdelsalam, P. N. Bartlett and A. E. Russell, *Nano Letters*, 2005, **5**, 2262-2267.
17. X.-M. Lin, Y. Cui, Y.-H. Xu, B. Ren and Z.-Q. Tian, *Analytical and Bioanalytical Chemistry*, 2009, **394**, 1729-1745.
18. F. S. Ou, M. Hu, I. Naumov, A. Kim, W. Wu, A. M. Bratkovsky, X. Li, R. S. Williams and Z. Li, *Nano Letters*, 2011, **11**, 2538-2542.
19. E. C. Le Ru, E. Blackie, M. Meyer and P. G. Etchegoin, *The Journal of Physical Chemistry C*, 2007, **111**, 13794-13803.
20. N. Leopold, V. Chiş, N. E. Mircescu, O. T. Marişca, O. M. Buja, L. F. Leopold, C. Socaciu, C. Braicu, A. Irimie and I. Berindan-Neagoe, *Colloids and Surfaces A: Physicochemical and Engineering Aspects*, 2013, **436**, 133-138.
21. H. Wang, C. S. Levin and N. J. Halas, *Journal of the American Chemical Society*, 2005, **127**, 14992-14993.
22. L. He, J. Huang, T. Xu, L. Chen, K. Zhang, S. Han, Y. He and S. T. Lee, *Journal of Materials Chemistry*, 2012, **22**, 1370-1374.
23. M.-W. Shao, M.-L. Zhang, N.-B. Wong, D. D.-d. Ma, H. Wang, W. Chen and S.-T. Lee, *Applied Physics Letters*, 2008, **93**, 233118.
24. X. T. Wang, W. S. Shi, G. W. She, L. X. Mu and S. T. Lee, *Applied Physics Letters*, 2010, **96**, 053104.
25. J.-A. Huang, Y.-Q. Zhao, X.-J. Zhang, L.-F. He, T.-L. Wong, Y.-S. Chui, W.-J. Zhang and S.-T. Lee, *Nano Letters*, 2013, **13**, 5039-5045.
26. M. Peng, H. Xu and M. Shao, *Applied Physics Letters*, 2014, **104**, 193103.
27. B. Zhang, H. Wang, L. Lu, K. Ai, G. Zhang and X. Cheng, Advanced Functional Materials, 2008, **18**, 2348-2355.
28. J. Huang, F. Chen, Q. Zhang, Y. Zhan, D. Ma, K, Xu and Y. Zhao, ACS Applied Materials & Interfaces, 2015, **7**, 10, 5725-5735.
29. C.-Y. Chen, L.-J. Hsu, P.-H. Hsiao and C.-T. R. Yu, Applied Surface Science, 2015, **355**, 197-202.
30. H.-J. Ahn, P. Thiyagarajan, L. Jia, S.-I. Kim, J.-C. Yoon, E. L. Thomas and J.-H. Jang, *Nanoscale*, 2013, **5**, 1836-1842.
31. J. Theiss, P. Pavaskar, P. M. Echternach, R. E. Muller and S. B. Cronin, *Nano Letters*, 2010, **10**, 2749-2754.
32. J. T. Bahns, A. Imre, V. K. Vlasko-Vlasov, J. Pearson, J. M. Hiller, L. H. Chen and U. Welp, *Applied Physics Letters*, 2007, **91**, 081104.
33. R. Alvarez-Puebla, B. Cui, J.-P. Bravo-Vasquez, T. Veres and H. Fenniri, *The Journal of Physical Chemistry C*, 2007, **111**, 6720-6723.
34. S. J. Lee, A. R. Morrill and M. Moskovits, *Journal of the American Chemical Society*, 2006, **128**, 2200-2201.
35. M. Hu, F. S. Ou, W. Wu, I. Naumov, X. Li, A. M. Bratkovsky, R. S. Williams and Z. Li, *Journal of the American Chemical Society*, 2010, **132**, 12820-12822.
36. M. S. Schmidt, J. Hübner and A. Boisen, *Advanced Materials*, 2012, **24**, OP11-OP18.
37. J. F. Betz, W. W. Yu, Y. Cheng, I. M. White and G. W. Rubloff, *Physical Chemistry Chemical Physics*, 2014, **16**, 2224-2239.
38. N. R. Jana and T. Pal, *Advanced Materials*, 2007, **19**, 1761-1765.
39. L. Tong, T. Zhu and Z. Liu, *Chemical Society Reviews*, 2011, **40**, 1296-1304.
40. X. Li and P. W. Bohn, *Appl. Phys. Lett.*, 2000, **77**, 2572-2574.
41. W.-K. To, C.-H. Tsang, H.-H. Li and Z. Huang, *Nano Letters*, 2011, **11**, 5252-5258.
42. M.-L. Zhang, K.-Q. Peng, X. Fan, J.-S. Jie, R.-Q. Zhang, S.-T. Lee and N.-B. Wong, *The Journal of Physical Chemistry C*, 2008, **112**, 4444-4450.
43. Z. Huang, N. Geyer, P. Werner, J. de Boor and U. Gösele, *Advanced Materials*, 2011, **23**, 285-308.
44. D. Kumar, S. K. Srivastava, P. K. Singh, K. N. Sood, V. N. Singh, N. Dilawar, M. Husain, J*ournal of Nanoparticle Research,* 2010, **12** 2267-2276.
45. P. Singh, S. K. Srivastava, M. Yameen, B. Sivaiah, V. Prajapati, P. Prathap, S. Laxmi, B. P. Singh, Vandana, C. M. S. Rauthan, P. K. Singh J*ournal of Materials Science*, 2015, **50**, 6631-6641.
46. S. K. Srivastava, D. Kumar, S. W. Schmitt, K. N. Sood, S. H. Christiansen and P. K. Singh, *Nanotechnology*, 2014, **25**, 175601
47. E. Garnett and P. Yang, *Nano Letters*, 2010, **10**, 1082-1087.
48. Huang, Jian-An and Zhao, Ying-Qi and Zhang, Xue-Jin and Luo, Lin-Bao and Liu, Yan-Kuan, Zapien, Juan Antonio, Surya, Charles, Lee and Shuit-Tong, *Applied Physics Letters*, 2011, **98**, 183108.

49. N. Bontempi, M. Salmistraro, M. Ferroni, L. E. Depero and I. Alessandri, *Nanotechnology*, 2014, **25**, 465705.
50. D. Kumar, S. K. Srivastava, P. K. Singh, K. N. Sood, V. N. Singh, N. Dilawar and M. Husain, Journal of Nanoparticles Research, 2010, **12**, 6, 2267-2276.
51. R. L. M. Dobson, S. Motlagh, M. Quijano, R. T. Cambron, T. R. Baker, A. M. Pullen, B. T. Regg, A. S. Bigalow-Kern, T. Vennard, A. Fix, R. Reimschuessel, G. Overmann, Y. Shan and G. P. Daston, *Toxicological Sciences*, 2008, **106**, 251-262.
52. C. Chartier, S. Bastide and C. Lévy-Clément, Electrochimica Acta, 2008, **53**, 5509-5516.
53. S. L. Cheng, C. H. Chung and H. C. Lee, *Journal of The Electrochemical Society*, 2008, **155**, D711-D714.
54. K. Seo, M. Wober, P. Steinvurzel, E. Schonbrun, Y. Dan, T. Ellenbogen and K. B. Crozier, *Nano Letters*, 2011, **11**, 1851-1856.
55. F. Silly, A. Q. Shaw, M. R. Castell, G. A. D. Briggs, M. Mura, N. Martsinovich and L. Kantorovich, *The Journal of Physical Chemistry C*, 2008, **112**, 11476-11480.
56. M. Mura, N. Martsinovich and L. Kantorovich, *Nanotechnology*, 2008, **19**, 465704.
57. E. Koglin, B. J. Kip and R. J. Meier, *The Journal of Physical Chemistry*, 1996, **100**, 5078-5089.
58. B. Liu, M. Lin and H. Li, *Sensing and Instrumentation for Food Quality and Safety*, 2010, **4**, 13-19.
59. Z.-Q. Wen, G. Li and D. Ren, *Appl. Spectrosc.*, 2011, **65**, 514-521.
60. A. M. Giovannozzi, F. Rolle, M. Sega, M. C. Abete, D. Marchis and A. M. Rossi, *Food Chemistry*, 2014, **159**, 250-256.
61. K. Wu, T. Rindzevicius, M. S. Schmidt, K. B. Mogensen, S. Xiao and A. Boisen, Optics Express, 2015, **23**, 10, 12965-12978.
62. [Codex Alimentarius Commission, Geneva, Switzerland, 5–9 July 2010, Report on the Thirty-Third Session of the Joint FAO/WHO Food Standards Programme.

Journal Name

ARTICLE

Figures

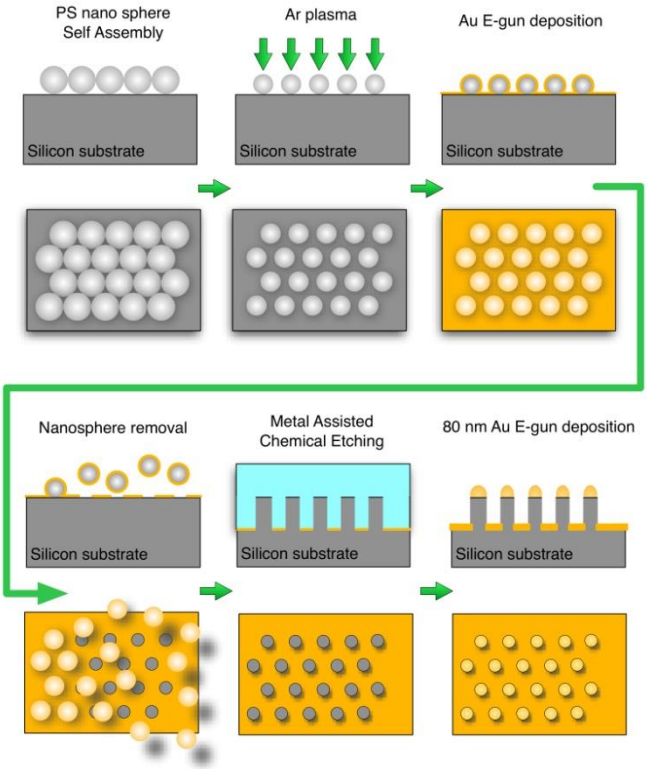

Fig.1 Scheme of SiNWs fabrication. The original spheres are 260 nm, the SiNWs 100 nm in diameter and 1 µm -1.3 µm in height.

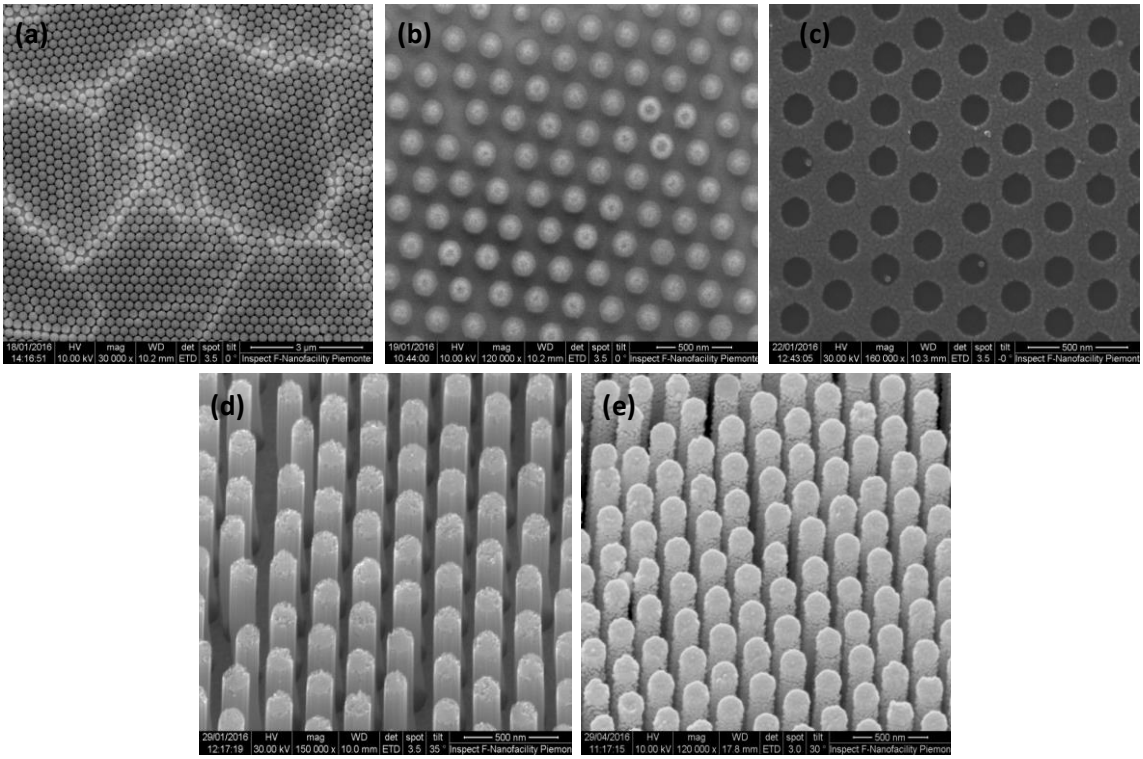

Fig. 2 SEM images reporting consecutive steps of fabrication. (a) monolayer of PS nanospheres self-ordered in hcp configuration in domains of some micrometers. (b) PS reduced nanospheres. (c) Au thin film patterned with circular voids resulting after reduction of the nanospheres and their removal. (d) Resulting matrix of SiNWs. (e) SiNWs covered with 80 nm of gold.

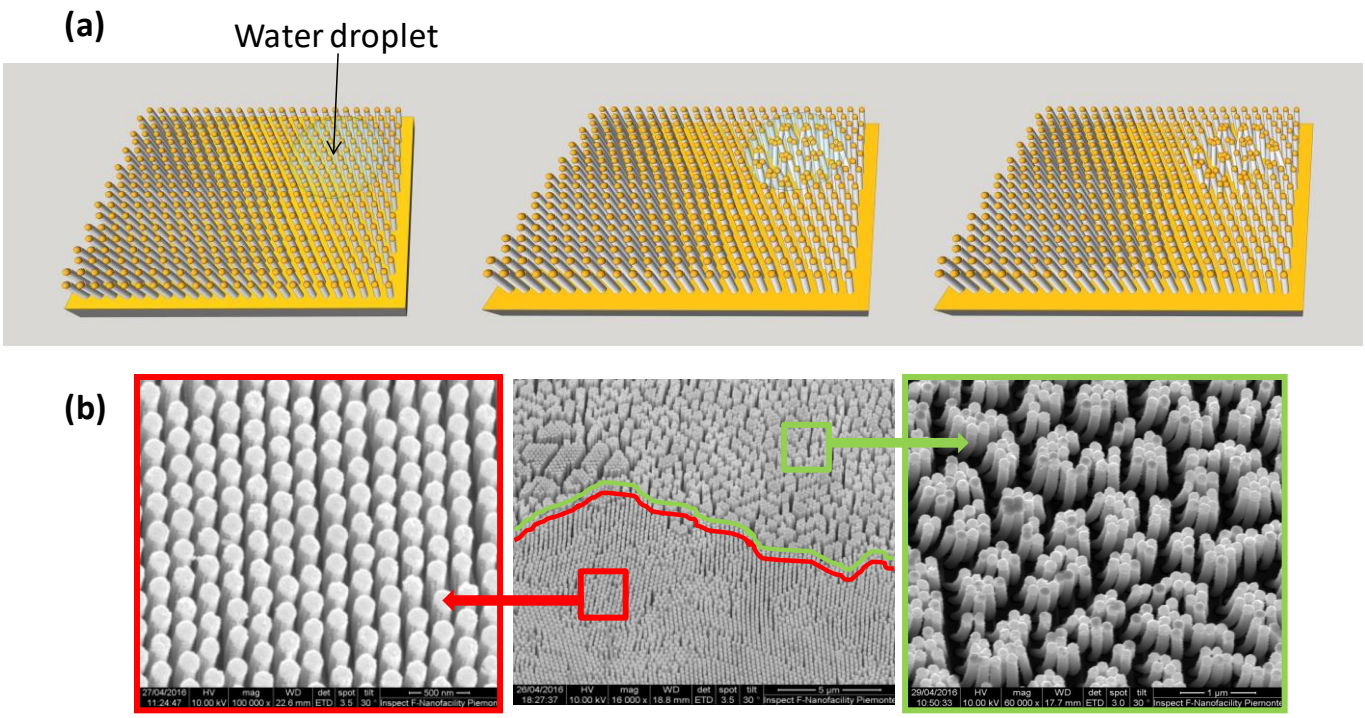

Fig. 3 (a) Illustration of the leaning of the SiNWs during the water evaporation. (b) SEM images of SiNWs after water evaporation within (green area) and outside (red area) the droplet region.

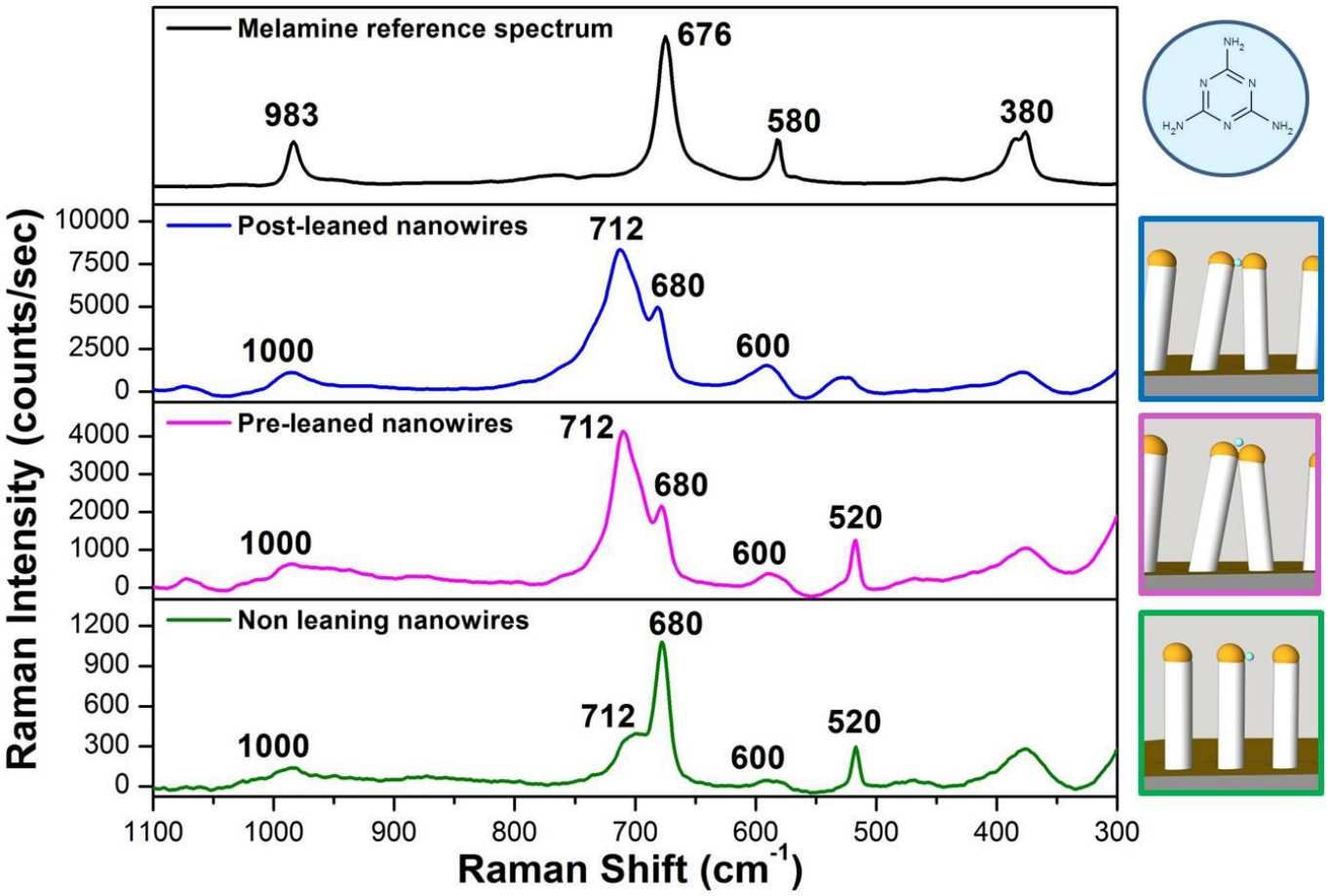

Fig. 4 Reference Raman spectrum of melamine powder with main assignments in the spectral region 300 cm^{-1} – 1100 cm^{-1} (black line). Raman spectra recorded from post-leaned nanowires (blue line), pre-leaned nanowires (violet line) and non leaning nanowires (green line) after the deposition of a 1 µl droplet of a 100 mg l^{-1} Mel solution on each substrate. Raman measurements were performed in air after the evaporation of the solvent.

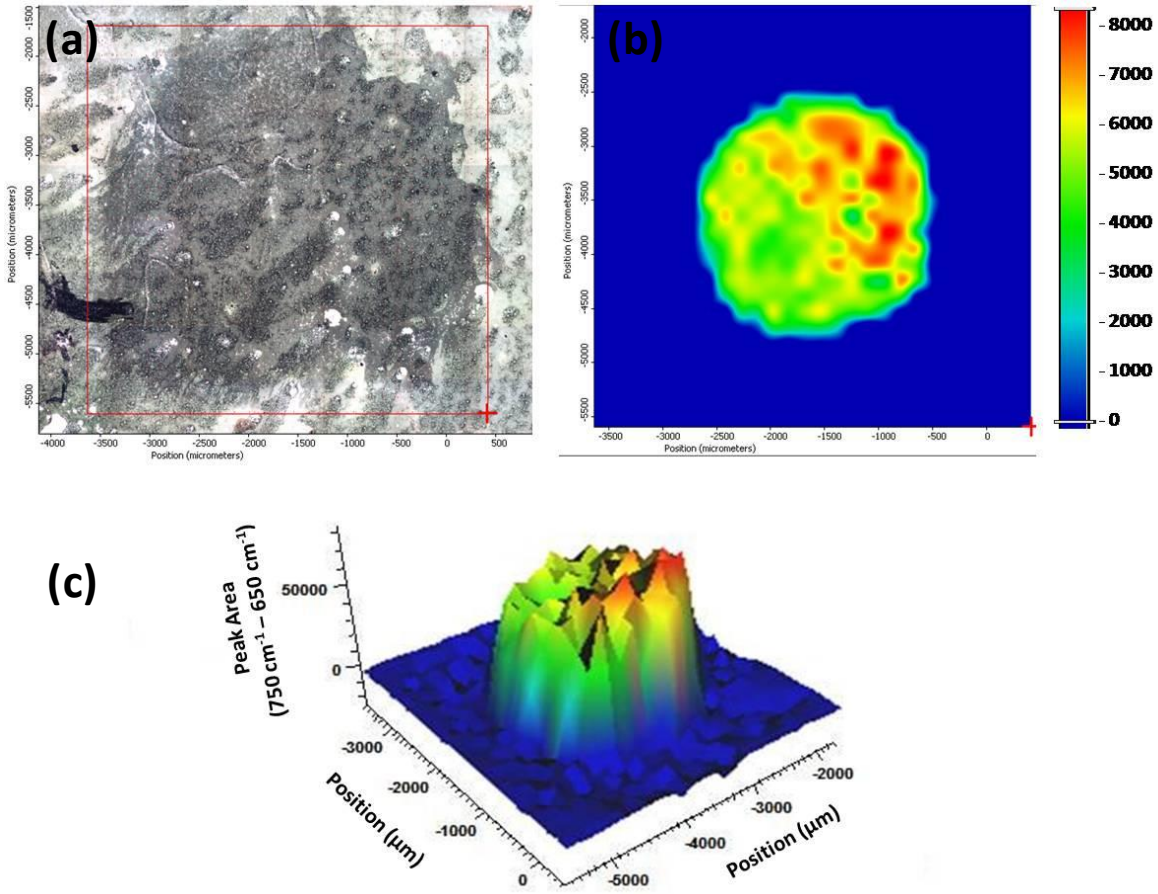

Fig. 5 (a) Optical image of SiNWs substrate after the deposition of a 1 µl droplet of a 100 mg l^{-1} Mel solution. The darker region on the image clearly identifies the post-leaned nanowires area obtained after the evaporation of the solution. (b) Raman map of the optical image shown in a) which was obtained by plotting the area of the specific Mel peak in the spectral range 750 cm^{-1} – 650 cm^{-1} across the analyzed surface of the SiNWs substrate. A color scale bar from blue to red provides semi quantitative analysis. c) 3D representation of the Raman map in b).

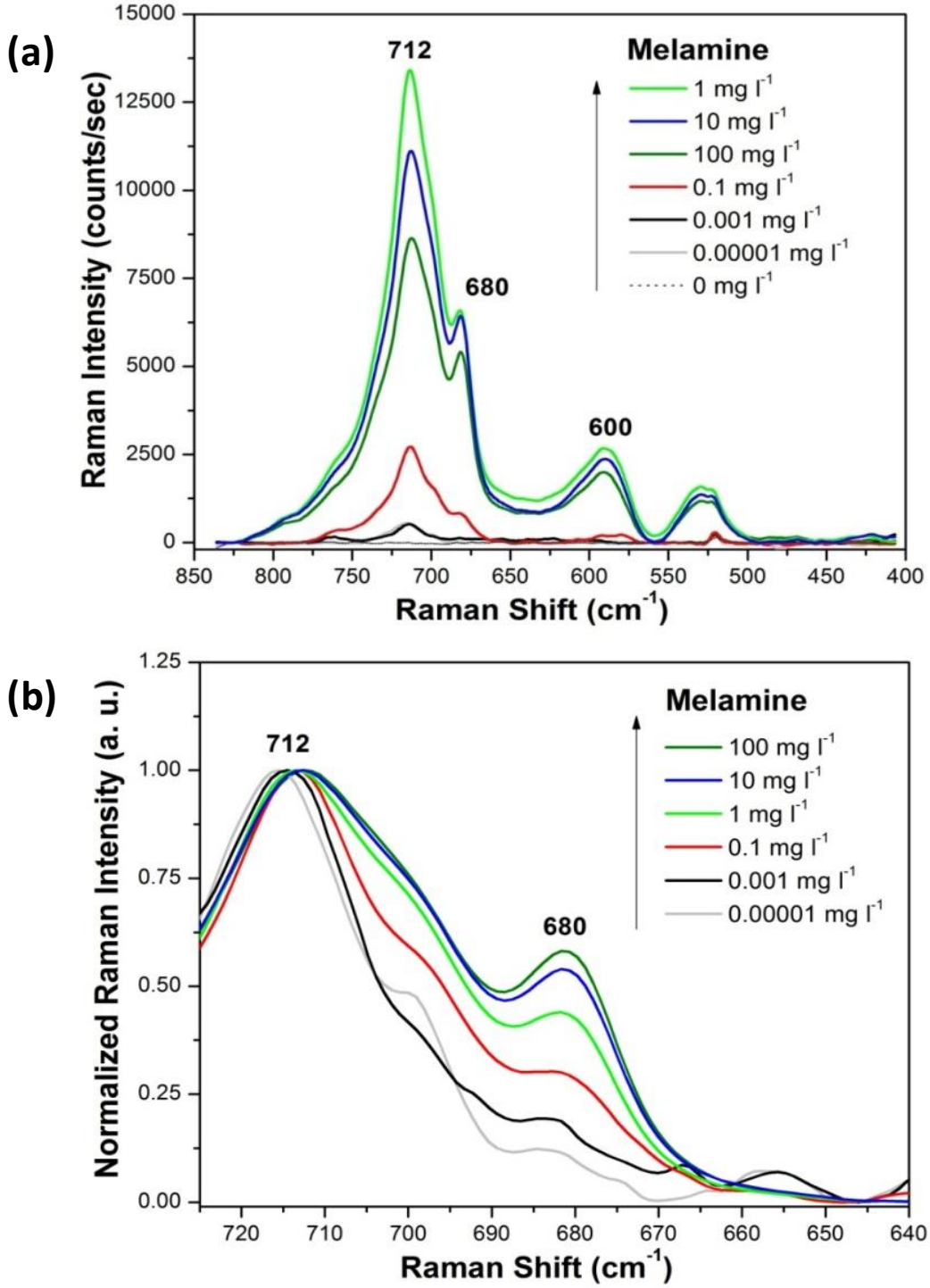

Fig. 6 (a) Raman spectra recorded from post-leaned nanowires substrates after the deposition of a 1 µl droplet of Mel solutions at 100 mg l^{-1}, 10 mg l^{-1}, 1 mg l^{-1},0.1 mg l^{-1}, 0.001 mg l^{-1} and 0.00001 mg l^{-1}.Raman measurements were performed in air after the evaporation of the solvent, (b) Normalization of the Raman spectra from to the intensity of the peak at 712 cm^{-1}. The intensity ratio at 680 cm^{-1} tends to increase proportionally with the melamine concentration.

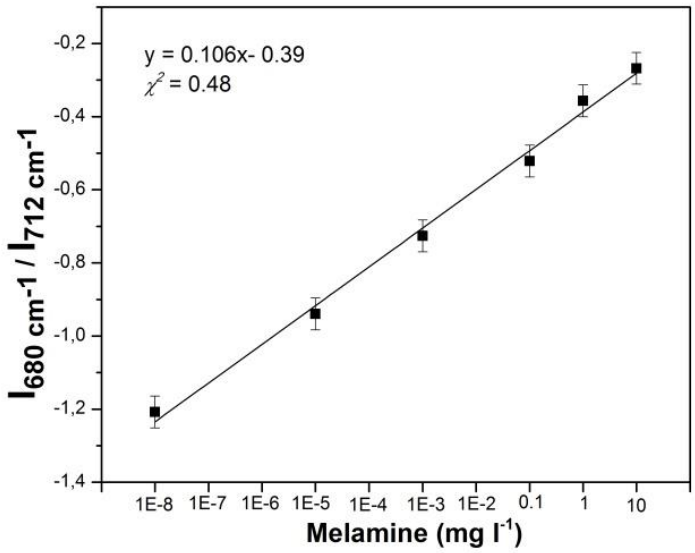

Fig. 7 Calibration curve obtained by plotting the logarithm of the relative intensity ratio at 680 cm^{-1}/ 712 cm^{-1} with the logarithm of Mel concentration in the range $1*10^{-8}$ mg l^{-1} - 10 mg l^{-1}.